Plasmonic interactions between a perforated gold film and a thin gold film*

Zhou Xin(周 昕)[a)b)], Li Hong-Jian(李宏建)[a)b)†], Xie Su-Xia(谢素霞)[a)b)], Fu Shao-Li(付少丽)[a)], Xu Hai-Qing(徐海清)[a)], and Wu Jin-Jun(吴金军)[a)]

[a)] *College of Physics Science and Technology, Central South University, Changsha* 410083, *China*
[b)] *College of Materials Science and Engineering, Central South University, Changsha* 410083, *China*

(Received 31 January 2010; revised manuscript received 5 April 2010)

Based on the finite difference time domain method, we investigated theoretically the optical properties and the plasmonic interactions between a gold film perforated with periodic sub-wavelength holes and a thin gold film. We showed that the plasmon resonant energies and intensities depend strongly on the thicknesses of the two films and the lattice constant. Based on the distributions of normal electric field component E_z, tangential electric field component E_y and total energy, we showed that the optical transmission is due to the collaboration of the localized waveguide resonance, the surface plasmon resonance and the coupling of the flat-surface plasmon of the two layers.

Keywords: plasmonic interaction, localized waveguide resonance, surface plasmon resonance, surface plasmon coupling

PACC: 7850J, 7820P, 7320J

1. Introduction

When the electromagnetic wave irradiates on a metal surface, driven by the high frequency electric field, free electrons on the metal surface may oscillate accordingly. The interaction between the surface charge oscillation and the electromagnetic field of the light generates a surface wave known as surface plasmon (SP).[1,2] Plasmon can be excited in the structure that is built in free-electron-like metal such as Au and Ag on or near the metal surface, when the light frequency matches the frequency of collective oscillations of the conduction electrons. Plasmon provides a powerful means of confining light to metal/dielectric interfaces, which in turn can generate intense local electromagnetic fields and significantly amplify the signal derived from analysis techniques that rely on light, such as surface enhanced Raman scattering and negative refraction.[3−5] There are also potential applications in building optical filters and sensors, as well as ultrasmall waveguides depending on subwavelength plasmonic structures as potential optical interconnects in computer chips.[6−9]

Plasmonic behaviour is a physical concept that describes the collective oscillation of conduction electrons in a metal (or a doped semiconductor) and is known through extensive theoretical and experimental studies. One outstanding example is the extraordinary transmission of light through a metallic film perforated by an array of subwavelength holes, which is attributed to the resonant excitation of surface plasmon polaritons set up by the periodicity of the array at the in-plane metal surfaces.[10−13] It is widely accepted that this enhanced transmission is due to the resonant coupling between the incident light and the surface plasmon excited on the metal-dielectric boundary of the periodic structure through evanescent wave. Recent explanations for the enhancement phenomenon are the collaboration of localized waveguide resonance with surface plasmon resonance.[2,14−16]

In this paper, using the finite difference time domain (FDTD) method, we investigated the optical properties of a gold film perforated with periodic arrays of sub-wavelength rectangular holes on top of a thin gold film (the perforated-film/film system). In contrast to the periodic arrays of sub-wavelength holes in a metallic film, the perforated-film/film system shows more resonant peaks. This means the system we studied possesses more plasmon resonance modes at the same time. Moreover, in the perforated-film/film

*Project supported by the National Natural Science Foundation of China (Grant No. 60708014), the Science Foundation for Postdoctorate of China (Grant No. 2004035083), the Natural Science Foundation of Hunan Province of China (Grant No. 06JJ2034), the Excellent Doctorate Dissertation Foundation of Central South University (Grant No. 2008yb039) and the Hunan Provincial Innovation Foundation for Postgraduate (Grant No. CX2009B029).

†Corresponding author. E-mail: lihj398@ yahoo.com.cn

© 2010 Chinese Physical Society and IOP Publishing Ltd

system, the transmission spectra show all forbidden bands between the resonant peaks. It proves that the system has better filtering and frequency-selecting characteristics than the monolayer perforated Au film. Based on the distributions of normal electric field component E_z, tangential electric field component E_y and total energy, we show that these resonant peaks may be attributed to three different resonant features and their coupling with each other: one is the localized waveguide resonance where the air hole can be considered as a truncated rectangular with both ends open to free space, the second is the surface plasmon resonance due to the periodicity of arrays, and the third is the coupling of the flat-surface plasmons of the two layers.

2. Model and theory

The three-dimensional (3D) finite difference time domain (FDTD) method[17] is employed to simulate the transmission spectra and the distribution of the filed intensity of the perforated-film/film system. The dispersion properties of the metal must be considered here since the absorption and permittivity of the metallic material are frequency-dependent. The Drude model is used to describe the dependence of the metallic permittivity on the frequency:[18,19]

$$\varepsilon_{\mathrm{m}}(\omega) = \varepsilon_{\infty}\left(1 - \frac{\omega_{\mathrm{p}}^2}{\omega(\omega + \mathrm{i}\gamma)}\right), \tag{1}$$

where ω is the angular frequency of the incident wave, ε_0 the permittivity of vacuum, $\omega_{\mathrm{p}} = 1.374 \times 10^{16}$ s^{-1} is the bulk plasma frequency of the gold, and $1/\gamma_{\mathrm{p}} =$ 245 fs represents the damping rate which characterizes the Ohmic absorption loss.

Light propagation in the metal can be described by the Maxwell's equations, which are coupled with the oscillations of quasi-free electrons (Drude model):[19]

$$\begin{aligned} \boldsymbol{\nabla} \times \boldsymbol{E} &= -\mu_0 \frac{\partial \boldsymbol{H}}{\partial t}, \\ \boldsymbol{\nabla} \times \boldsymbol{H} &= -\varepsilon_0 \frac{\partial \boldsymbol{E}}{\partial t} + \boldsymbol{J}, \\ \frac{\partial \boldsymbol{J}}{\partial T} &+ \gamma \boldsymbol{J} = \varepsilon_0 \omega_{\mathrm{p}}^2 \boldsymbol{E}, \end{aligned} \tag{2}$$

where $\boldsymbol{E}$ and $\boldsymbol{H}$ are the electric and magnetic field vectors, respectively. $\boldsymbol{J}$ is the current density and equals the time derivative of the metal polarization, i.e., $\boldsymbol{J} = \partial \boldsymbol{P}/\partial t$. μ_0 is the magnetic permeability of vacuum.

We consider a periodic array of rectangular apertures perforated on a gold film which has the layer spacing $d = 20$ nm with the second gold film as shown schematically in Figs. 1(a) and 1(b). In all the cases, light is normal-incident to the surface. We assume that the upper perforated film's thickness is $h = 0.08a$ and the rectangular apertures has the sides $b_x = 0.792a$ and $b_y = 0.176a$, where $a = 250$ nm. In addition, the lattice constant is $a_0 = a$. In Fig. 1(b), we can see that the input light wave is polarized along the short edge of the rectangular holes (the y direction) and propagates along the z direction. Moreover, periodic boundary conditions are imposed on the four surfaces in the holes perpendicular to each gold film. Perfectly matched layers are imposed at the left and right surfaces of each layer. Geometric variable h_1 represents the thickness of the second gold film. We studied the transmission spectra and energy distribution when the receiving surface is set at the midpoint of the perforated-film/film system.

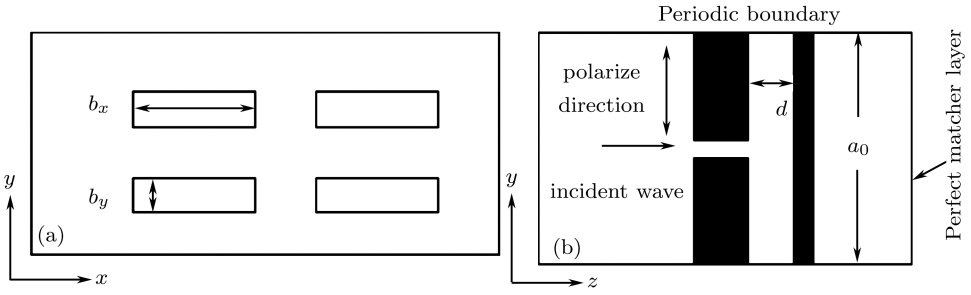


Fig. 1. Schematic illustrations of the perforated-film/film system. (a) Top view of the structure, the rectangular air-holes of sides b_x and b_y are perforated on a freestanding gold film of thickness h for upper layer. (b) The yz cross section of the computational domain consisting of a single unit cell of the double-layer films. A normal incident light wave polarized along the y direction, periodic boundary conditions are imposed on the four surfaces perpendicular to the gold film, while perfect matched layers are imposed at the left and right surfaces.

It is well known that at the interface separating a metal and a dielectric, the SP mode obeys the following dispersion relation:

$$|\boldsymbol{k}_{\rm sp}| = |\boldsymbol{k}_0|\sqrt{\frac{\varepsilon_1\varepsilon_2}{\varepsilon_1+\varepsilon_2}}, \tag{3}$$

where $\boldsymbol{k}_{\rm sp}$ and $\boldsymbol{k}_0$ are the surface plasmon wave vector and the wave vector of the incident light, ε_1 and ε_2 are the dielectric constants of the incident medium (air here) and the metal films, respectively. For the normal incidence, the wavelengths of the excited surface plasmon resonance modes are given approximately by $\lambda_{\max}$ as follows:

$$\lambda_{\max}(m,n) \cong \frac{a_0}{\sqrt{m^2+n^2}}\sqrt{\frac{\varepsilon_1\varepsilon_2}{\varepsilon_1+\varepsilon_2}}, \tag{4}$$

where integers m and n denote the number of half wave variations in the x and y directions, respectively, ε_1 is the dielectric constant of the interface medium, and ε_2 is that of the metal. Therefore, the transmission peaks can be indexed with integers (m,n) in the optical spectra.

3. Results and discussion

In Fig. 2, we show the transmission spectra in the cases of the structure with different h_1, the thickness of the second gold film. In the single-layer gold hole array transmission spectrum ($h_1 = 0$ nm), the two transmission peaks which correspond to the excitation of SP modes are observed at 0.424 μm with a transmission of 0.857, and at 0.737 μm with a transmission of 0.91. The anomalous transmission means that not only the electromagnetic energy impinging directly on the hole gets transmitted but also part of the energy shining on the gold surface is converted into transmission, and such transmission peaks are attributed to the surface plasmon at the metal–air interface. However, the number of transmission peaks increases from two to four and the intensities of transmission peaks weaken markedly when we add the second gold film. The added peaks are attributed to the additional localized surface plasmon resonance (see Fig. 4) and the flat-surface plasmons coupling on the perforated-fim/film interface (see Fig. 6) after adding the second Au film, see below for further information. The intensities of transmission peaks decrease when the number of Au layer is increased due to the absorption of Au and the scattering and reflection.[20] Furthermore, in the perforated-film/film system transmission spectra, there appear some forbidden bands between the resonant peaks. Similarly, almost no light wave can transmit at a wavelength longer than the last peak position. Along with the thickness of the second gold film (h_1) increasing, the peaks of the plasmon resonances all have a slight blueshift and the intensities of peaks reduced gradually. For example, when the thickness is increased to $h_1 = 50$ nm from $h_1 = 20$ nm, the resonance wavelength near the higher photonic band edge (shown by vertical dotted line in Fig. 2) is shifted to 0.764 μm from 0.776 μm and the intensity is weakened to 0.0847 from 0.3447. When the second gold film thickness is increased, the energy required for driving the resonant oscillation increased, this phenomenon may result in a spectral blueshift. In addition, the transmission bandwidths of the four resonances are quite different. The two low-energy (long wavelength) transmission resonances are always wider than the two high-energy transmission resonances. More interestingly, from both transmission spectra in Fig. 2 one can find the cutoff wavelength region around 250 nm corresponding to Wood's anomaly which should occur at wavelength $\lambda = a_0$.[21]

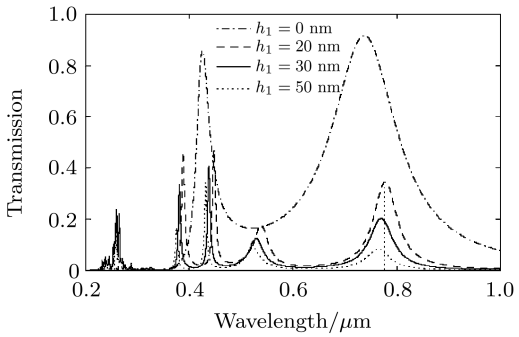


Fig. 2. The transmittances for the perforated-film/film system with different second film thickness $h_1 = 0$, 20, 30, and 50 nm.

To reveal the physical mechanism behind the resonance peaks, we will discuss the spatial distributions of mechanism of electric field for the broken line ($h_1 = 20$ nm) in Fig. 2, in which the resonance peaks correspond to 0.776 μm, 0.539 μm, 0.448 μm and 0.388 μm in turn from right to left. These modes may mean many different couplings of surface plasmons, and we can get more information about the resonant modes through describing the electric field distribution. Figures 3(a) and 3(b) show the normal electric field components E_z and tangential electric field components E_y at wavelength 0.776 μm for the perforated-film/film system in the y–z plane respectively. According to the boundary condition $\boldsymbol{n}\cdot\boldsymbol{E} = \sigma/\varepsilon_0$, where

σ is the surface charge density and the normal direction $\boldsymbol{n} = n\boldsymbol{z}$, we are able to determine the magnitude of surface charges σ through detecting $|E_z|$.[22,23] From Fig. 3(a), we can see the positive and negative charge densities (labeled with + and –) as measured by the normal electric field E_z tend to accumulate at the metal corners. Abundant charges is located between the first perforated film and the second gold film but there is no charge at the part corresponding to the hole between the layers. Additionally, charge signs between the two layers are opposite to the input side of the first layer. We obtained a periodic distribution of surface charge which is consistent with the local charge dipole oscillation in the direction perpendicular to the long edges of the rectangular air holes. Seemingly, the hole behaves like a dipole and the "dipole" is flanged by opposite surface charges and these periodic charges establish a standing wave resonance in the rectangular air hole region. The local charge dipole oscillation is also revealed from the tangential electric field component E_y that is entirely localized in the air hole region (as shown in Fig. 3(b)). E_y, which is nearly a standing wave inside the hole of the first perforated layer, is negative. The resonance mode at wavelength 0.776 μm originates from the localized surface plasmon resonance and it does not fell the modulation of the surface structure periodicity on the xy plane. So each air hole in the first perforated film can be considered as a truncated rectangular waveguide with four metal walls and two sides open to free space. The truncated waveguide forms a low-quality resonator. It is dependent on the hole shape but almost independent of the period of the structure.[24] Additionally, even if the gold film is very thin the waveguide resonance exists, which can be expressed as the Febry-perot effect.[14,25]

The total energy distribution of the electric and the magnetic field at wavelength 0.776 μm is obtained in the yz plane as shown in Fig. 3(c). We can clearly see that the total energy is mostly concentrated inside the hole and the layer space. It seems the total energy distribution in the layer space is larger than that in the hole, which may be due to the stronger surface plasmon coupling between the layers.

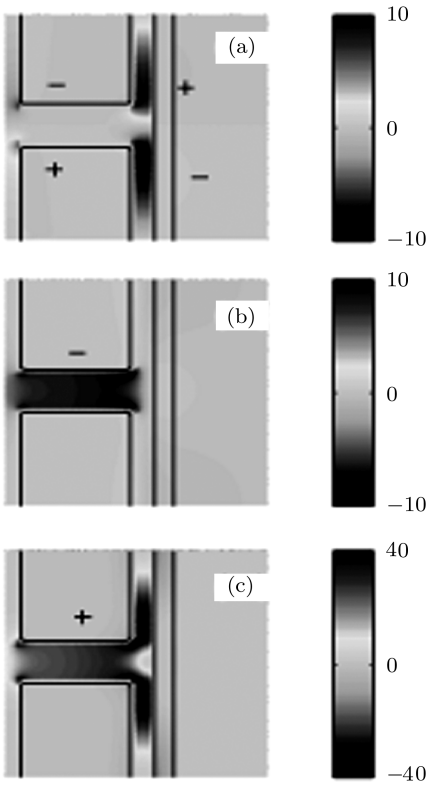


Fig. 3. The yz cross section for the amplitude evaluated at the resonant wavelength 0.776 μm of (a) the normal electric field component E_z distribution, (b) the tangential electric field component E_y distribution, and (c) the total energy distribution of magnetic and electric fields.

Figures 4(a), 4(b), and 4(c) show the normal electric field components E_z, the tangential electric field components E_y, and the total energy distribution of the calculation results for magnetic and electric fields wavelength 0.539 μm for the perforated-film/film system in the y–z plane, respectively. There is only one difference between Fig. 4(a) and Fig. 3(a), that is, the charge signs between the two layers for the latter are the same as the input side of the first layer. The tangential electric field component E_y concentrates mostly in the hole region whereas almost no E_y energy distributes between the two layers (as shown in Fig. 4(b)). Moreover, the intensity of the E_y energy reduces gradually from the entrance of the hole and almost vanishes at the rearward of the hole. Eventually, the total energy distribution at wavelength 0.539 μm (as shown in Fig. 4(c)) is seen to be entirely localized inside the hole and the two layers, meanwhile the intensity decays gradually from the entrance of the hole to the space between the two layers. The resonance peak is located at the wavelength of 0.539 μm, which also exhibits the dipole oscillation behaviour and can be attributed to the localized surface plasmon resonance.

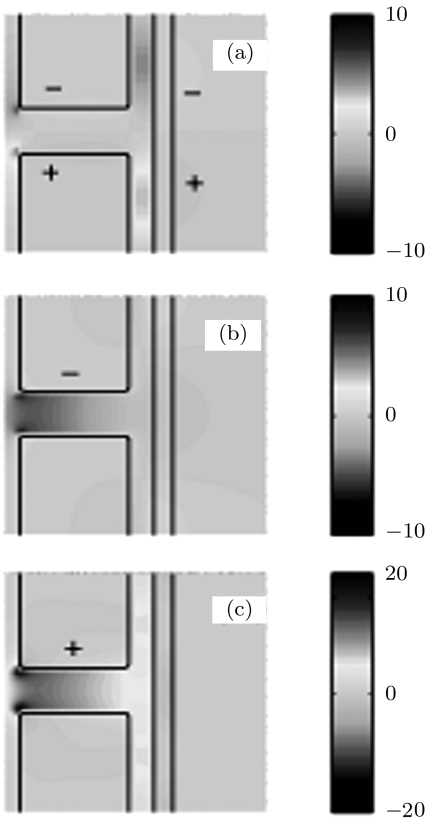


Fig. 4. The yz cross section for the amplitude evaluated at the resonant wavelength 0.539 μm of (a) the normal electric field component E_z distribution, (b) the tangential electric field component E_y distribution, and (c) the total energy distribution of magnetic and electric fields.

In Figs. 5(a), 5(b), and 5(c) , we show the normal electric fields E_z, the tangential electric field components E_y, and the total energy distributions at the peak transmission wavelength 0.448 μm. As was known,[14,25] the surface plasmon mode originates from the well-recognized surface plasmon structure-factor-induced resonance effect. The positive and negative charge densities (labeled with + and –) as measured by the normal electric field E_z can extend to the metal regions between the holes in Fig. 5(a). However, the charge densities at the corners are much higher than that in metal walls regions, which is a typical edge effect. As can be seen, the signs of charge densities at the entrance of the rectangular hole are the same as those between the two layers, which is opposite to that of Fig. 3(a). Coupling of the surface charges in the region between the two layers can be observed. We obtained a periodic distribution of surface charges (labeled with + and –) and such a distribution is consistent with the local charge dipole oscillations that establish a standing wave resonance along y direction inside the rectangular air hole. The local charge dipole oscillation is also revealed from the tangential electric field component E_y. For the first perforated layer, E_y is seen to be entirely localized around the two open ends of the nanohole, and it is positive inside the holes near the entrance interface, while negative at the exit side. Instructive coupling of the surface plasmon with different signs is expected. The tangential electric filed E_y is localized separately on the two surfaces, indicating that this resonance mode is formed due to the well-recognized surface structure periodicity. The electromagnetic energy simulation result shown in Fig. 5(c) shows that the total energy is strongly located between the two layers, however, for the air hole, intensity of energy is weakened greatly. One can observe that the energy shown in Fig. 5(c) is larger than that in other figures, which correspond to the highest peak of the perforated-film/film system resonance spectra in Fig. 2.

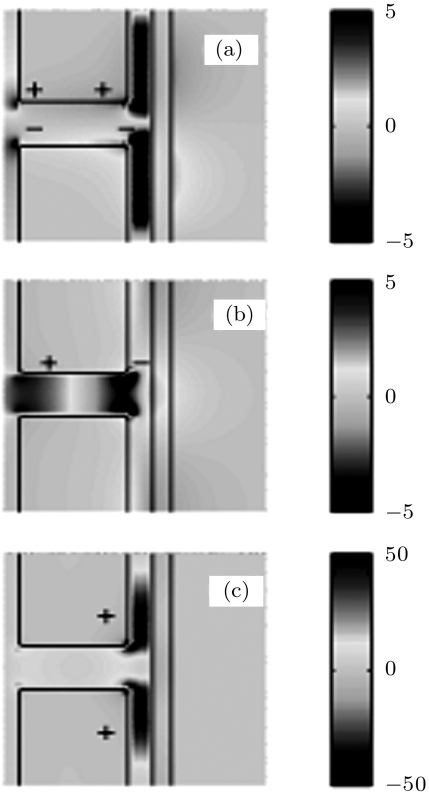


Fig. 5. The yz cross section for the amplitude evaluated at the resonant wavelength 0.448 μm of (a) the normal electric field component E_z distribution, (b) the tangential electric field component E_y distribution, and (c) the total energy distribution of magnetic and electric fields.

Interestingly, the electric fields and total energy distributions at the peak resonance wavelength 0.388 μm (see Figs. 6(a), 6(b) and 6(c)) are very different from other figures. From Fig. 6(a), it can be seen that the positive and negative surface charges are alternately arranged along the metal hole walls down to the end of the hole. Whereas, there appear pos-

itive and negative charge groups assembled between the lower and upper space of the two layers, respectively. This demonstrates that the energy transmits along the metal hole wall by dipole oscillation. We also obtained the E_y distribution that negative charge located inside the air hole and positive–negative charges alternately located between the spaces of the two layers, which is just opposite to the E_z distribution shown in Fig. 6(b). The total energy distribution at wavelength 0.539 μm is still seen to be localized inside the hole and the space between two layers, but it seemed that there is a fraction of energy embedded in the film which leads to the total energy form barbell shape between the two layers. This resonance peak may come from both the flat-surface plasmons on the perforated-fim/film interface and the strong coupling of the SPs. From all that discussed above, we can see that the perforated-film/film system has four plasmon coupling modes. The localized waveguide resonance and the well-recognized surface plasmon resonance due to the periodicity are consistent with the monolayer perforated metallic film. However, there are also peculiar coupling modes (localized surface plasmon resonance and the flat-surface plasmons coupling) corresponding to the two additional transmission peaks.

The first perforated film thickness h also plays an important role in determining the plasmon resonance wavelength of the perforated-film/film system. For the second gold film with the same thickness $h_1 = 20$ nm, the transmission spectra are shown in Fig. 7 for different first perforated film thickness $h = 75$, 107 and 200 nm. There still appear four resonance peaks when the changes are very large. The resonance peak with the longest wavenumber is blueshifted but the other three peaks are red-shifted when h increases. Especially, the transmission peak at around 0.6 μm has a larger shift and the intensity reduces and the bandwidth increases with h increasing. While the intensities of other resonance peaks basically enhance as h increases. So, the first perforated film thickness h strongly affects the characters of the perforated-film/film system, which results from that the thickness affects the interactions of the surface plasmons.

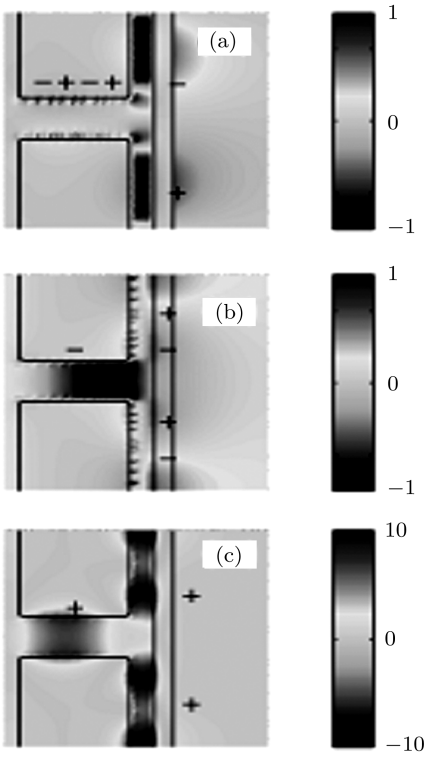


Fig. 6. The yz cross section for the amplitude evaluated at the resonant wavelength 0.388 μm of (a) the normal electric field component E_z distribution, (b) the tangential electric field component E_y distribution, and (c) the total energy distribution of magnetic and electric fields.

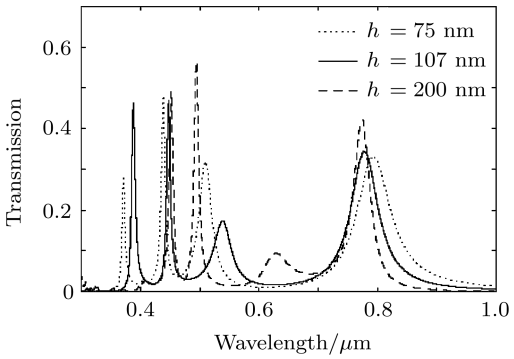


Fig. 7. The transmission for the perforated-film/film system with different first perforated film thickness $h = 75$, 107 and 200 nm.

In order to investigate the role of the lattice constants on the transmission spectra, the cases of three different lattice constants ($a_0 = 0.9a$, $1a$ and $1.1a$) while the other parameters ($h = 107$ nm, $h_1 = 20$ nm) are fixed, are investigated, and the calculation results are shown in Fig. 8. All the resonance peaks are redshifted obviously, at the same time the intensities of the peaks are strengthened along with the lattice constant a_0 increasing. This means that the resonant excitation modes of surface plasmons become steadier. From Figs. 2, 7 and 8, we can know that the coupling of SPs strongly depends on the structure of

the perforated-film/film system, which makes it possible to adjust the location and quality factor of the mode, and so on. These features can be applied to tune electromagnetic wave in sub-wavelength optoelectronic devices.

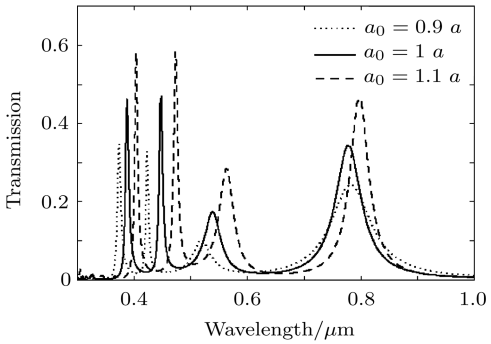


Fig. 8. Normalized transmission for the perforated-film/film system with different lattice constants $a_0 = 0.9a$, $1a$ and $1.1a$.

4. Conclusions

In summary, we have investigated the optical transmission properties of the perforated-film/film system. We showed that the plasmon resonance energies and intensities depend strongly on the thicknesses of perforated film and the second metallic film and the lattice constant. The plasmon resonance coupling inside and outside the holes enhances the field at two openings of the hole in the perforated-film/film system. Therefore, the plasmonic interactions play an important role on transmission enhancement through the perforated-film/film system. The transmission spectra, charge density, and tangential electric field of the resonant state are used to characterize the different resonances.

References

[1] Genet C and Ebbesen T W 2007 *Nature* (London) **445** 39

[2] Tang Z H, Peng R W, Wang Z, Wu X, Bao Y J, Wang Q J, Zhang Z J, Sun W H and Wang M 2007 *Phys. Rev.* B **76** 195405

[3] Bozhevolnyi S I, Volkov E D V S, Laluet J Y and Ebbeson T W 2006 *Nature* (London) **440** 508

[4] Ma J Y, Xu C, Liu S J, Zhang D W, Jin Y X, Fan Z X and Shao J D 2009 *Chin. Phys.* B **18** 1029

[5] Zou S L and Schatz G C 2005 *Chem. Phys. Lett.* **403** 62

[6] Genet C and Ebbesen T W 2007 *Nature* (Landon) **445** 39

[7] Barnes W L, Dereux A and Ebbesen T W 2003 *Nature* (London) **424** 824

[8] Maier S A and Atwater H A 2005 *J. Appl. Phys.* **98** 011101

[9] Zayats A V and Smolyaninov I I 2003 *J. Opt.* A: *Pure Appl. Opt.* **5** S16

[10] Veselago V G 1968 *Sov. Phys. Usp.* **10** 509

[11] Pendry J B, Holden A J, Robbins D J and Stewart W J 1999 *IEEE Trans. Microwave Theor. Tech.* **47** 2075

[12] Ebbesen T W, Lezec H J, Ghaemi H F, Thio T and Wolff P A 1998 *Nature* (London) **391** 667

[13] Shelby R A, Smith D R and Schultz S 2001 *Science* **292** 77

[14] Ruan Z C and Qiu M 2006 *Phys. Rev. Lett.* **96** 233901

[15] Li H J, Xie S X, Zhou R L, Liu Q, Zhou X and Yuan M 2008 *J. Phys.*: *Condens. Matter* **20** 415223

[16] Chen Y G, Wang Y H, Zhang Y and Liu S T 2007 *Opt. Commun.* **274** 236

[17] Taflove A and Hagness S C 2000 *Computational Electrodynamics*: *The Finite-Difference Time-Domain Method* 2nd. edn. (Norwood: Artech House INC)

[18] Baida F I and Van Labeke D 2003 *Phys. Rev.* B **67** 155314

[19] Müller R, Malyarchuk V and Lienau C 2003 *Phys. Rev.* B **68** 205415

[20] Tang Z H, Peng R W, Wang Z, Wu X, Bao Y J, Wang Q J, Zhang Z J, Sun W H and Wang M 2007 *Phys. Rev.* B **76** 195405

[21] Wood R W 1902 *Proc. R. Soc. London* A **18** 269

[22] García N and Nieto-Vesperinas M 2007 *J. Opt.* A: *Pure Appl. Opt.* **9** 490

[23] Huang X R, Peng R W, Wang Z, Gao F and Jiang S S 2007 *Phys. Rev.* A **76** 035802

[24] Palik E D 1991 *Handbook of Optical Constants in Solids* (Boston: Academic) Vol. 1

[25] Hou B, Mei J, Ke M Z, Wen W J, Liu Z Y, Shi J and Sheng P 2007 *Phys. Rev.* B **76** 054303

[26] Beruete M, Sorolla M, Campillo I, Dolado J S, Martin-Moreno L, Bravo-Abad J and Garcia-Vidal F J 2005 *IEEE Trans. Antennas Propag.* **53** 1897